Propagation of singularities in shells of non-uniform geometrical nature. A numerical investigation

Fabien Béchet

Propagation of singularities in shells of non-uniform geometrical nature. A numerical investigation.

F. Béchet [a]

[a] *LAMIH UMR CNRS 8201, Polytechnical University of Hauts-de-France, Le Mount Houy, 59313 Valenciennes cedex 9, France*

Abstract

This paper deals with the propagation of singularities in thin elastic shells whose middle surface is not of an uniform nature. Numerical computations are performed using an adaptive mesh procedure proposed by the software Abaqus to refine the mesh inside the internal layers. The computation are done on three kinds of shells: hyperbolic-parabolic, hyperbolic-elliptic and parabolic-elliptic. The numerical results enable us to determine the propagation of singularities in such shells and to have information about their nature. In particular, when a singular force is applied in the hyperbolic part of a shell, the numerical computations show that a singularity propagates in the hyperbolic part and that a reflection occurs at the boundary with a part of a different nature (parabolic or elliptic).

Key words: Shell theory, Singular perturbation, Adaptive mesh, Internal layers

1. Introduction

This paper is concerned with the propagation of singularities in thin elastic shells having a non-uniform geometrical nature. A shell is 3D solid whose one dimension (the thickness h) is much smaller than the two other dimensions. Classically, the geometry of a shell is described by a middle surface S and a value of the thickness h for each point of the surface. In this paper, we consider shells with a constant thickness h. A point p of a surface S can be classified with respect to the signs of the principal curvatures of the surface at this point: the point is parabolic (FIG. 1) when one and only one of its principal curvature vanishes, hyperbolic (FIG. 2) when the principal curvatures are of a different sign and elliptic (FIG. 3) when the principal curvatures have the same sign [1]. If all the points of the surface have the same nature, respectively parabolic, hyperbolic or elliptic the surface is said respectively parabolic, hyperbolic or elliptic. By extension, the corresponding shell is said parabolic, hyperbolic or elliptic. In this paper, we will focus on shells which do not have an uniform nature. The three possible combinations are considered: hyperbolic/parabolic, hyperbolic/elliptic and parabolic/elliptic.

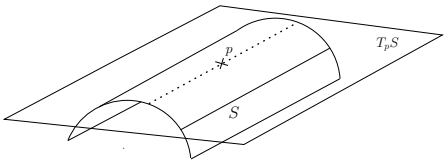

Figure 1. Parabolic point

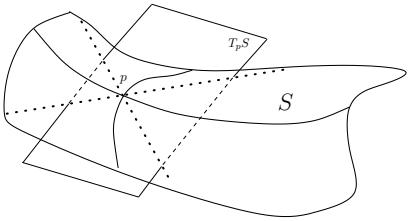

Figure 2. Hyperbolic point

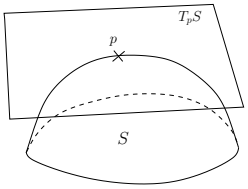

Figure 3. Elliptic point

Classically, when mechanical models of thin shell are deduced from the three-dimensional elasticity by asymptotic methods with the relative thickness $\varepsilon = h/L_c$ as small parameter (L_c is a charateristic length of the middle surface), we obtain at the limit for $\varepsilon = 0$ either a membrane model [2] or a pure bending model [3] if the shell is respectively geometrically rigid or not.

The Koiter shell model [4], which couples both membrane and bending effects, can not be obtained from three-dimensional elasticity by asymptotic methods. However, it was shown that its asymptotic behaviour is good for both possible limits (membrane or flexion) [5]. This is why this model is widely used for numerical computations. The classical variational formulation of the Koiter model in its nondimensional form (1) contains the membrane bi-linear form a_m proportional to 1 and the bending bi-linear form a_b proportional to ε^2. Other models contain shear effects like the Naghdi model or "s-m-b model" in [6] but the shear effects tend asymptotically to 0 when the relative thickness $\varepsilon \searrow 0$ and the limit problem is the same as the Koiter model. For $\varepsilon > 0$, the problem corresponding to the Koiter model is always elliptic and classical results of regularity hold true [7].

When $\varepsilon \searrow 0$, the limit problem of the Koiter shell model will be identical to that of the asymptotic limit of three-dimensional elasticity [5]. It depends on the space G of *inextensional displacements* which keep the metrics of the middle surface of the shell unchanged. If the space $G \neq \{0\}$, the shell is said *non-geometrically rigid* or equivalently *non-inhibited*. When $\varepsilon \searrow 0$, we have a *penalty problem* tending to the pure bending model [3]. Oppositely, if $G = \{0\}$, the shell is *geometrically rigid* or *inhibited*. We have a *singular perturbation* problem whose limit is the membrane model [2]. For a given shell, the inhibited character only depends on the boundary conditions. For any type of shells (parabolic, hyperbolic or elliptic), a sufficient condition to have $G = \{0\}$ is that all the boundaries are fixed or clampled. Detailed studies about the conditions necessary to have a geometrically rigid shell are presented in [8,9]. More complex cases occur for hyperbolic shells which can be "partially non-inhibited" as studied in Chapter 10 of [10].

The present paper is focused on inhibited shells. For such shells, the limit problem is the membrane problem. In many situations, the solution u^0 of the membrane model is singular because of the loading and/or the boundary conditions. The membrane model is less rich than the full problem and is not able to give a smooth solution where bending effects are important especially where the normal loadings are applied and near the clamped of fixed boundaries. The nature of the singularity (order, propagation) is directly related to the nature of the middle surface of the shell. In any case, the most singular component of the displacement is the displacement in the direction normal to the shell which is denoted u_3^0 at the limit $\varepsilon = 0$.

When $\varepsilon > 0$ (which is always the case for any physical problem), these singularities are replaced by internal layers and boundary layers which contain bending effects and most of the deformation energy. Such problems have been studied theoretically and numerically for parabolic, hyperbolic and elliptic shells in the case of a singular loading normal to the shell [10]. The results are very different whether the loading is singular along an asymptotic line of the middle surface or not. An asymptotic line is a line tangent to the asymptotic directions at every point. The asymptotic directions are the directions for which the normal curvature vanishes [1]. There are two asymptotic directions for hyperbolic points, 1 for parabolic points and

0 for elliptic points (see dotted lines in FIG. 1, FIG. 2 and FIG. 3). Thus, if the loading is normal and singular along an asymptotic line, we have:

— For parabolic shells: the singularities of the normal displacement u_3^0 are 4 orders more singular than the normal loading f^3 and propagate along the single family of asymptotic lines of the middle surface [11,12].

— For hyperbolic shells: the singularities of u_3^0 are only 2 orders more singular than the normal loading f^3 but propagate along the 2 families of asymptotic lines of the middle surface [13]. Moreover, a pseudo-reflection of the signularity occurs when a singularity reaches a boundary if this boundary is not parrallel to the asymptotic lines and clamped or fixed [14]. In that case, the pseudo-reflected singularity loses 1 order compared to the original one.

Studies have also been carried out on shells with a fold, both parts of the shell having the same geometrical nature [15]. It was shown that for parabolic shells, singularities propagate across the fold with the same order of singularity.

If the loading is singular along a non-asymptotic line, the singularity of the normal displacement u_3^0 is the same as the one of the normal loading and no propagation occurs. It means that the normal displacement u_3^0 is only singular where the loading is singular and with the same order of singularity. That is always the case for elliptic shells which have no asymptotic lines. However, other kinds of singularities may appear either if an elliptic shell is *well-inhibited* [16] or *ill-inhibited* [17,18,19,20].

In the literature, no paper is concerned with the propagation of singularities for shells with a non-uniform geometrical nature (parabolic, hyperbolic, elliptic). In this paper, we will study the propagation of singularities when the nature the shell is not the same at every point. We will consider cases without any fold: the nature of the middle surface will evolve smoothly without any discontinuities of the normal N.

The paper is organized as follows. In the first section, some recalls about the singular perturbation problem associated to the Koiter model and about singularities are presented. Then, the problem considered in this paper and the numerical method used are detailed. Finally, in the last three sections, the results of the numerical simulations are presented and analysed for three different types of shell: hyperbolic-parabolic (HP), hyperbolic-elliptic (HE) and parabolic-elliptic (PE) and two possible locations for the applied force (first part or second part). The first example denoted HP-H (HP shell with a force in the hyperbolic part) is presented in details whereas the other are presented more briefly.

2. Theory

In the present paper, the study is limited to linear elastic isotropic shells, whose behavior is described by the linear Koiter shell model [4]. We consider a shell whose middle surface is defined by the domain Ω and a mapping Ψ (see FIG. 4) and with a relative thickness $\varepsilon = h/L_c$ (the ratio of the thickness h of the shell to a characteristic length L_C of the middle surface).

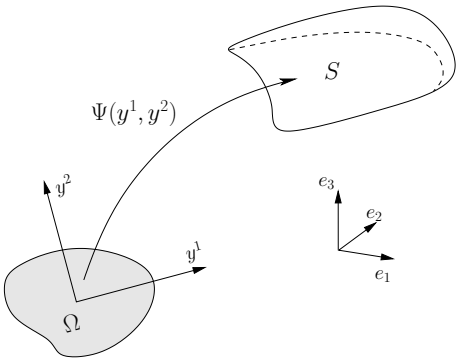

Figure 4. Mapping of the middle surface S

For a loading $\hat{f}$ applied on a part of the surface denoted S, the Koiter model classically writes in a dimensionless form:

$$\begin{gathered} Find\ u^\varepsilon\ \epsilon\ V,\ such\ as,\ \forall\ v\ \epsilon\ V: \\ a_m(u^\varepsilon, v) + \varepsilon^2 a_b(u^\varepsilon, v) = b(v) \end{gathered} \tag{1}$$

$$with\ \ V = \left\{ v = (v_1, v_2, v_3) \in H^1(\Omega) \times H^1(\Omega) \times H^2(\Omega) \right\}$$

satisfying the boundary kinematic conditions, where

$$a_m(u^\varepsilon, v) = \int_S A^{\alpha\beta\lambda\mu} \gamma_{\lambda\mu}(u^\varepsilon) \gamma_{\alpha\beta}(v) dS \tag{2}$$

and

$$a_b(u^\varepsilon, v) = \frac{1}{12} \int_S A^{\alpha\beta\lambda\mu} \rho_{\lambda\mu}(u^\varepsilon) \rho_{\alpha\beta}(v) dS \tag{3}$$

are respectively the membrane energy and the bending energy bilinear forms. The right-hand side

$$b(v) = \int_S f^i v_i dS \tag{4}$$

where we have set $\hat{f} = \varepsilon f$ denotes the work of applied forces due to the displacement v.

The components $\gamma_{\alpha\beta}$ and $\rho_{\alpha\beta}$ of the membrane strain tensor and of the tensor of curvature variation are respectively given by:

$$\gamma_{\alpha\beta}(u^\varepsilon) = \frac{1}{2}(D_\alpha u^\varepsilon_\beta + D_\beta u^\varepsilon_\alpha) - b_{\alpha\beta} u^\varepsilon_3 \tag{5}$$

and

$$\rho_{\alpha\beta}(u^\varepsilon) = \partial_\alpha \partial_\beta u^\varepsilon_3 - \Gamma^\gamma_{\alpha\beta} \partial_\gamma u^\varepsilon_3 - b^\gamma_\alpha b_{\gamma\beta} u^\varepsilon_3 + D_\alpha \left(b^\gamma_\beta u^\varepsilon_\gamma \right) + b^\gamma_\alpha D_\beta u^\varepsilon_\gamma \tag{6}$$

where

$$D_\alpha u^\varepsilon_\beta = \partial_\alpha u^\varepsilon_\beta - \Gamma^\lambda_{\alpha\beta} u^\varepsilon_\lambda \tag{7}$$

denotes the covariant derivative of u^ε_β, ∂_α being the classical derivative with respect to y^α and $\Gamma^\lambda_{\alpha\beta}$ the Christoffel symbols of the middle surface. Finally, $b_{\alpha\beta}$ are the coefficients of the second fundamental form of the middle surface accounting for curvatures.

The coefficients $A^{\alpha\beta\lambda\mu}$ are the coefficients of the linear elastic isotropic constitutive law. They represent a fourth order tensor given by:

$$A^{\alpha\beta\lambda\mu} = \frac{E}{2(1+\nu)}\left[a^{\alpha\lambda}a^{\beta\mu} + a^{\alpha\mu}a^{\beta\lambda} + \frac{2\nu}{1-\nu}a^{\alpha\beta}a^{\lambda\mu}\right] \tag{8}$$

where E and ν are the Young's modulus and the Poisson's ratio, and $a^{\alpha\beta}$ the contravariant components of the metric tensor.

Remark *In the present paper, the linear Koiter model is used (small displacements, linear Hooke's law). However, the displacements can in some cases be out of the linear range and the Von Mises stresses over the yield stress. But as we are interested in the qualitative results and not the value of displacements and stresses, it would always be possible to consider a loading αf^3 with $\alpha \ll 1$ leading to a normal displacement αu_3^ε in the linear range and a Von Mises stress below the yield stress.*

It is important to note that the membrane strain tensor $\gamma_{\alpha\beta}$ in (2) does not involve derivatives of the normal displacement u_3^ε whereas the tensor of curvature variation $\rho_{\alpha\beta}$ in (3) involves second order derivatives of u_3^ε.

When $\varepsilon \searrow 0$, the limit problem of the Koiter shell model (1) is very different either the space

$$G = \{v \in V;\ a_m(v,v) = 0\} = \{v \in V;\ \gamma_{\alpha\beta}(v) = 0\} \tag{9}$$

reduces to $\{0\}$ or not. The space G is the space of inextensional displacements which deform the middle surface without modifying its dimensions. When $G \neq \{0\}$, the shell is said "non-inhibited" and the limit problem is the pure bending one [3]. Oppositely, when $G = \{0\}$, the shell is *inhibited* or *geometrically rigid*. In this paper, this latter case will be considered. When $\varepsilon \searrow 0$, we have a singular perturbation problem whose limit is the membrane problem [2]:

$$\begin{gathered} Find\ u^0 \in V_a,\ such\ as,\ \forall\ v \in V_a : \\ a_m(u^0, v) = b(v) \end{gathered} \tag{10}$$

$$with\ \ V_a = \left\{v = (v_1, v_2, v_3) \in H^1(\Omega) \times H^1(\Omega) \times L^2(\Omega)\right\}$$

and satisfying the boundary conditions.

Problem (10) implies only the membrane strain tensor $\gamma_{\alpha\beta}$ and therefore lower order differential operators compared to problem (1). Consequently, the solutions (displacements and stresses) of this limit problem can be singular for very usual boundary conditions and for very usual loadings such as a point force normal to the shell or a constant pressure on a part of the shell.

During the singular perturbation problem (when $\varepsilon \searrow 0$), the regular solution u^ε tends to the singular solution u^0. The solution u^ε is always smooth: it contains boundary or internal layers where the solution u^0 is singular. Inside these layers, bending effects are still present even for small values of ε. The structure of the singularities arising in these layers is very different with respect to the geometrical nature of the shell.

The study of the singular perturbation process is classically done by using the limit problem (10) and determine the singularity of the solution u^0. The membrane model can be expressed in term of membrane stresses [9]:

$$\begin{cases} -D_\alpha T^{\alpha\beta} = f^\beta \quad in \quad \Omega \\ \\ -b_{\alpha\beta} T^{\alpha\beta} = f^3 \quad in \quad \Omega \end{cases} \tag{11}$$

with the constitutive law : $T^{\alpha\beta} = A^{\alpha\beta\lambda\mu}\gamma_{\lambda\mu}(u^0)$ and the associated boundary conditions.

An important result is that the characteristic lines of the differential system (11) are the asymptotic lines of the middle surface of the shell [9]. Consequently, the differential system is respectively parabolic, hyperbolic or elliptic if the middle surface of the shell is respectively parabolic, hyperbolic or elliptic.

For parabolic or hyperbolic shells, the most singular terms of the solution u^0 of the limit problem can be calculated (only the most singular term is important when $\varepsilon \searrow 0$) considering a well-adapted coordinate system where the curvature tensor reduces to one non-zero term. That was done in [12] for parabolic shells and in [13] for hyperbolic shells. For elliptic shells, the results were obtained in a different way [16].

For a given geometrical nature and loading, we want to determine the nature of the singularity of the solution u^0 of the limit problem. In particular, we want to predict:
— the order of the singularity compared to the order of singularity of the loading f (ex: a point force is a δ-like singularity in both directions)
— the possible propagation of this singularity
— the variation of the thickness η of the internal and boundary layers with respect to the relative thickness ε during the singular perturbation phenomenon.

Considering the case of a normal loading f^3 singular along a line, the main results are summarized in Table 1.

Properties	**Non asymptotic lines**	**Asymptotic lines**	
		hyperbolic	*parabolic*
singularity order of u_3^0 (compared to f^3)	+0	+2	+4
singularity order of u_1^0 and u_2^0 (compared to f^3)	-1 (or less)	+1 (or less)	+3 (or less)
propagation	no	yes	yes
layer thickness η	$\mathcal{O}(\varepsilon^{1/2})$	$\mathcal{O}(\varepsilon^{1/3})$	$\mathcal{O}(\varepsilon^{1/4})$

Table 1
Main results of the singularity orders of the displacements and of the thickness orders according to the considered case.

The singularities of the tangential displacements u_1^0 and u_2^0 are not well-defined because they depend on the problem considered and the coordinate system used whereas the normal displacement u_3^0 is always along the normal N to the middle surface and has always the same order of singularity compared to f^3.

According to the results of Table 1, when for instance a point force f^3 is applied at a point of a shell (it corresponds to a Dirac function δ), the normal displacement u_3^0 will have a singularity of the same order ($=\delta$) if the shell is elliptic, 2 orders higher ($= \delta^{(2)}$) if the shell is hyperbolic and 4 orders higher ($= \delta^{(4)}$) if the shell is parabolic, with propagation of the singularities along asymptotic lines for the two last cases. More details about the chain of singularities are given in section 2.1.

In this paper, we consider a shell having two parts: the first part has a certain geometrical nature (parabolic, hyperbolic or elliptic) and the second part has a different geometrical nature. We would like to know what happens when a singularity arising in one part (following the results of Table 1) propagates and reaches the border between the two parts: does the singularity propagate in the second part? What happens at the transition between the two parts?

The theoretical study is not an easy task. We can not study the propagation of the singularities between the two part using the well-adapted coordinate system as used for previous studies [11,13]. That is why this paper will mainly focus on numerical results to determine the behaviour of the singularities for such shells.

2.1. *Chain of singularities*

When considering functions (or distributions) of only one variable x, denoting by $S_0(x)$ a basic singularity, we will consider the corresponding chain of singularities:

$$\ldots,\ S_{-2}(x),\ S_{-1}(x),\ S_0(x),\ S_1(x),\ S_2(x),\ S_3(x),\ \ldots \tag{12}$$

with $S_{k+1} = \dfrac{d}{dx}\ S_k$. This chain must be understood in the sense of singular functions (or distributions) defined up to an additive function (or distribution) which is smooth in the neighbourhood of $x = 0$. A classical example of chain is

$$\ldots,\ xH(x)\ ,\ H(x),\ \delta(x),\ \delta'(x),\ \delta^{(2)}(x),\ \ldots \tag{13}$$

where $H(\cdot)$ is the Heaviside step function and $\delta(\cdot)$ the Dirac distribution. Other chains exist like in [12]. The Dirac family (13) is often met in thin shell problems because a point force corresponds to a Dirac distribution whereas a distributed force on a rectangular domain can be a represented with Heaviside step functions. The Dirac distribution can be seen as the limit when $\eta \searrow 0$ of a function having a support of width η and and amplitude $1/\eta$ with an integral equal to 1. For instance, we can see it as the limit of a Gaussian function

$$\frac{1}{\sqrt{\pi}\eta} e^{(-x/\eta)^2} \tag{14}$$

when $\eta \searrow 0$. Its derivative δ' is the limit of a function on the same support but with an amplitude $1/\eta^2$ and one more oscillation. The subsequent derivatives follows the same recursive rule. The n^{th} derivative of δ, denoted $\delta^{(n)}$ has an amplitude $1/\eta^{n+1}$ and $n+1$ main oscillations (FIG. 5). In practice, the number of oscillations is not easy to evaluate.

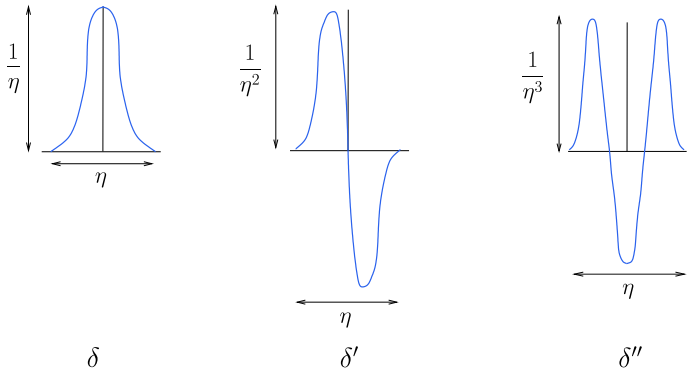

Figure 5. Properties of the Dirac family

In what follows, only the most singular term of the displacement will be considered since the lower order terms becomes negligible in comparison when $\varepsilon \searrow 0$.

Remark *For commodity, we will often use the term "singularity" for a function which is not singular but tending to a singular function when $\varepsilon \searrow 0$ like the example (14). The normal displacement u_3^ε is never singular but its limit u_3^0 is. The nature of the singularities of u_3^0 will be studied through the evolution of u_3^ε (amplitude, thickness η like presented in FIG. 5) inside the internal layers .*

3. Problem considered and numerical procedure used

3.1. *Geometry of the shell and properties of the middle surface*

In the sequel, we will consider revolution shells whose middle surface S is defined by the local mapping (Ω, Ψ) with:

$$\Psi(y^1, y^2) = \left(y^1, R(y^1)\sin\left(y^2\right), R(y^1)\cos\left(y^2\right)\right), \quad (y^1, y^2) \in \Omega \tag{15}$$

The domain Ω and the function $R(y^1)$ will be specified for three different types of shell. The covariant basis of the surface is defined by $a_\alpha = \partial_\alpha \psi$:

$$a_1 = \begin{pmatrix} 1 \\ \\ R'(y^1)\sin\left(y^2\right) \\ \\ R'(y^1)\cos\left(y^2\right) \end{pmatrix} \qquad a_2 = \begin{pmatrix} 0 \\ \\ R(y^1)\cos\left(y^2\right) \\ \\ -R(y^1)\sin\left(y^2\right) \end{pmatrix} \qquad N = \frac{1}{\sqrt{1+R'(y^1)^2}} \begin{pmatrix} -R'(y^1) \\ \\ \sin\left(y^2\right) \\ \\ \cos\left(y^2\right) \end{pmatrix} \tag{16}$$

The corresponding metric tensor writes:

$$a_{\alpha\beta} = \begin{pmatrix} 1+(R')^2 & 0 \\ \\ 0 & R^2 \end{pmatrix} \tag{17}$$

The tensor of curvatures writes:

$$b_{\alpha\beta} = \frac{1}{\sqrt{1+(R')^2}} \begin{pmatrix} R'' & 0 \\ \\ 0 & -R \end{pmatrix} \tag{18}$$

The functions $R(y^1)$ used in the sequel are chosen such that the curvatures b_{11} and b_{22} are continuous with respect to y^1. The sign of determinant of $b_{\alpha\beta}$

$$det(b) = \frac{-RR''}{1+R'^2} \tag{19}$$

gives the nature of the surface. As the function R chosen is positive, the sign of R'' gives the nature of the surface:

— for $R'' > 0$, $det(b) < 0$: the surface is hyperbolic.
— for $R'' = 0$, $det(b) = 0$: the surface is parabolic.
— for $R'' < 0$, $det(b) > 0$: the surface is elliptic.

At each point of the surface, the asymptotic directions vanish the second fundamental form $b_{11}(dy^1)^2 + b_{22}(dy^2)^2 + 2b_{12}dy^1dy^2$. This leads to two possible asymptotic directions:

$$dy^2 = \pm\sqrt{\frac{-b_{11}}{b_{22}}}dy^1 = \pm\sqrt{\frac{R''}{R}}dy^1 \tag{20}$$

which are distinct if the surface is hyperbolic ($b_{11}b_{22} < 0$), identical and corresponding to the lines $y^2 = 0$ if the shell is parabolic ($b_{11} = 0$) and imaginary if the shell is elliptic ($b_{11}b_{22} > 0$).

3.2. *Numerical procedure*

Numerical computations are performed with the software Abaqus [21], using the element STRI65 (triangle with quadratic interpolation, 5 degrees of freedom: 3 displacements and 2 rotations). It is based on the bending strain mesure of Budiansky-Sander shell model [22] which slightly differs from the Koiter's model in the expression (6) of the curvature variation tensor $\rho_{\alpha\beta}$. The element is adapted to thin shells: the Kirchhoff's condition is imposed numerically at certain points.

Predicting the propagation of singularities is not an easy task. Even when one can predict them, meshing the shell in a appropriate way is a fastidious task: one has to refine the mesh inside the layers, which can follow curved lines. That is why we will use adaptive meshes. That technique is available in Abaqus. A first uniform mesh is given. The results obtained with this first mesh are used to refine or coarse the mesh considering a criteria (Abaqus proposes the Von Mises stress or the deformation energy). A second computation is done and the process is repeated until the maximal error allowed is reached or up to a chosen maximum number of iterations.

For a fixed number of elements, adaptive meshes give better results than uniform meshes. The use of anisotropic adaptive meshes is the technique the most adapted to study boundary and internal layers [23] but it is not available in Abaqus.

In the sequel, six different cases will be considered. Three different middle surfaces combining 2 of the 3 types of surface will be studied (hyperbolic/parabolic, hyperbolic/elliptic, parabolic/elliptic). For each geometry, a normal force f^3 will be applied in the first part of the shell and then in the second part. For each case, numerical computations will be performed for different relative thicknesses ε from 10^{-4} to 10^{-7} in order to study the singular perturbation process and evaluate the singularities of the normal displacement appearing when $\varepsilon \searrow 0$.

4. Hyperbolic-Parabolic shell

4.1. *The shell considered and its geometrical properties*

First, we shall consider an example of a shell with a hyperbolic part and a parabolic part. The middle surface of the shell is defined by the local mapping (Ω, Ψ) given in (15) with $\Omega = [-L, L] \times [-\pi/2, \pi/2]$ and

$$\begin{cases} R(y^1) = \rho\left(1 - \left(\dfrac{y^1}{L}\right)^3\right) & \text{for } \; y^1 \epsilon\, [-L, 0[\\ \\ R(y^1) = \rho & \text{for } \; y^1 \epsilon\, [0, L] \end{cases} \tag{21}$$

The part of the shell corresponding to $y^1 < 0$ is hyperbolic whereas the part of the surface corresponding to $y^1 \geq 0$ is parabolic (this is a half cylinder). The surface is plotted on FIG. 6. With the function $R(y^1)$ chosen in (21), there is no fold: the normal is continuous with respect to y^1 at the "transition" $y^1 = 0$.

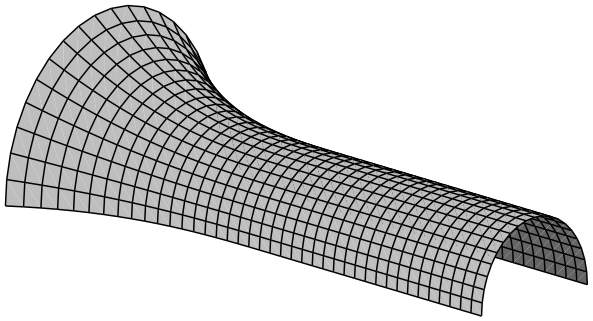

Figure 6. Middle surface of the HP shell

L	25 mm
ρ	100 mm
Young's modulus E	210 GPa
Poission's ratio ν	0.3

Table 2
Data used for the HP shell

The constants ρ and L denote respectively the radius and the length of the cylinder. For the HP shell, the characteristic length is taken as $L_C = 0.20525\ m$ (the length of the line $y^2 = 0$). The data used for the computations are summarized in Table 2. When nothing is specified, the relative thickness of the shell is $\varepsilon = 10^{-6}$.

Boundary conditions
The shell is clamped at all its boundary except along the line segment ($y^1 = L,\ y^2 = [0; \pi/2]$). Thus, the shell is inhibited (all the asymptotic lines are clamped at least in one point).

Loading
Two cases will be addressed. For both cases, a normal point force, proportional to the relative thickness $\tilde{f}^3 = -0.01 \times \varepsilon\ N$ (corresponding to $f^3 = -0.01\ N$ in equation (4)), is applied, in the hyperbolic part for the case HP-H or in the parabolic case for the case HP-P.

4.2. *Normal force $\tilde{f}^3$ applied in the hyperbolic part (case HP-H)*

Let us consider the normal point force $\tilde{f}^3$ is applied at the point $P = (-L/2, 0)$ in the plane of parameters, in the hyperbolic part. Since the shell is hyperbolic, two asymptotic lines passes through point P: they are obtained by integration from (20) (numerically for $y^1 < 0$) and plotted on FIG. 7 in the plane of parameters (y^1, y^2) and on FIG. 8 in the 3D space. They will be denoted AL_1 (blue line) and AL_2 (red line).

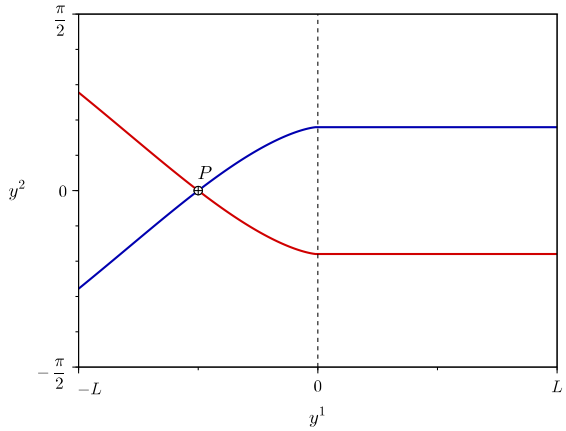

Figure 7. Case HP-H: The asymptotic lines passing through the point P in the plane of parameters.

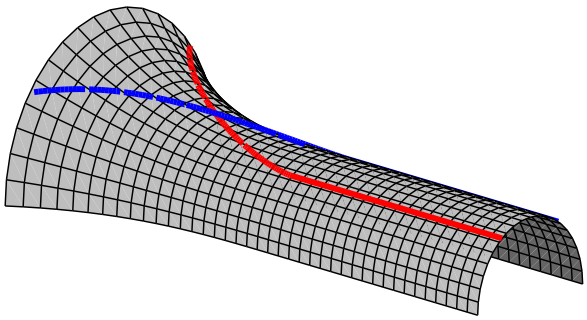

Figure 8. Case HP-H: The asymptotic lines passing through the point $\Psi(-\frac{1}{2}L, 0)$ in the 3D space.

Using the theoretical results of Table 1, the singular displacement caused by the point force at point P should propagate along the asymptotic lines passing through point P at least in the hyperbolic part. At the transition with parabolic part at $y^1 = 0$, we can postulate that the singularities will continue to propagate along the two asymptotic lines in the parabolic part but one does not know with which characteristics.

First, let us look at the remeshing process. Then, we will focus on the results and on the singular perturbation process.

4.2.1. *Mesh adaptation process for* $\varepsilon = 10^{-6}$

The evolution of the mesh during the adaptive remeshing is presented on figures 9 to 12 for the computation performed with $\varepsilon = 10^{-6}$. The remeshing was based on the Von Mises stress (uniform error distribution) and limited to 6 iterations (5 remeshings). At the end of the last iteration the chosen criteria of 4% of error was not satisfied.

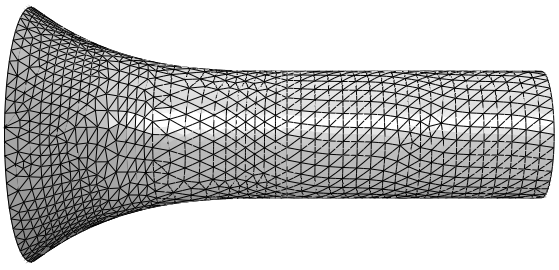

Figure 9. Case HP-H: Initial uniform mesh (1,741 elements)

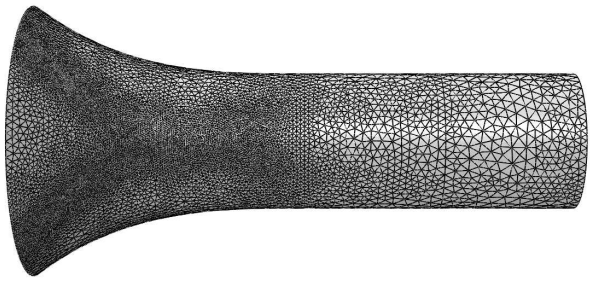

Figure 10. Case HP-H: Mesh of the 2^{nd} iteration (16,577 elements) for $\varepsilon = 10^{-6}$

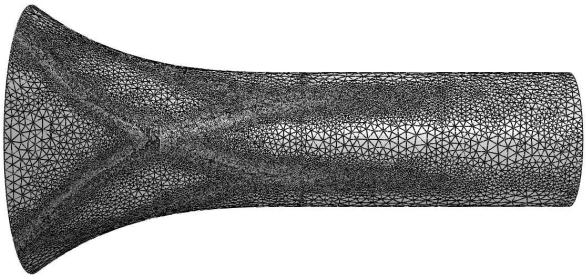

Figure 11. Case HP-H: Mesh of the 4^{th} iteration (240,856 elements) for $\varepsilon = 10^{-6}$

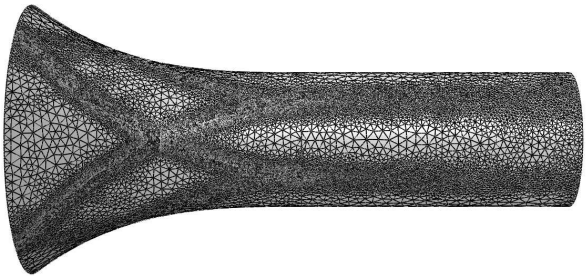

Figure 12. Case HP-H: Mesh of the 6^{th} iteration (302,406 elements) for $\varepsilon = 10^{-6}$

During the mesh adaptation process, the number of elements increases. The mesh is refined inside layers, and especially internal layers. The mesh is refined along the two asymptotic lines described on FIG. 7 and FIG. 8. But it is also refined along the following curves (FIG. 13):

(i) the 2 other asymptotic lines of the surface AL'_1 and AL'_2 passing through the points P_1 and P_2, intersections between the asymptotic lines AL_1 and AL_2 and the line $y^1 = 0$ (the transition between hyperbolic and parabolic parts).

(ii) the 2 other asymptotic lines of the surface AL''_1 and AL''_2 passing through the point P'_1 and P'_2, intersections between the asymptotic lines AL_1 and AL_2 and the boundary $y^1 = -L$ in the hyperbolic part.

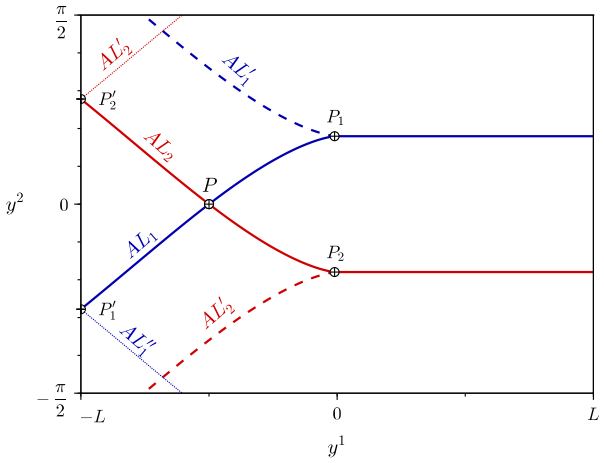

Figure 13. Case HP-H: Asymptotic lines bearing singularities

The evolution of the results of u_3^ε obtained with the successive meshes and for $\varepsilon = 10^{-6}$ are presented on Figures 14 to 17 on different lines. With the initial mesh, the singularities are nearly invisible. In the hyperbolic part, the results have converged at the 4^{th} iteration (FIG. 14). More iterations are needed in the parabolic part (FIG. 17). This is due to the amplitudes of the singularities which are much lower in the parabolic part. Then, the mesh is refined slower in this part of the shell.

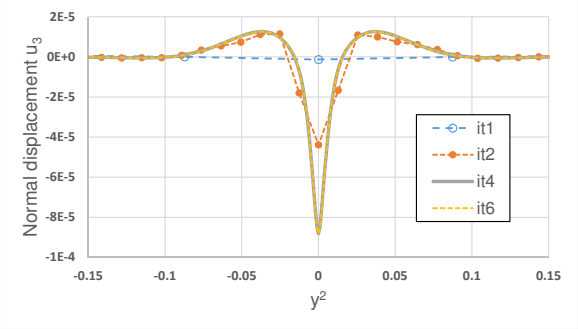

Figure 14. Case HP-H: Evolution of u_3^ε on the line $y^2 = -\frac{L}{2}$ during the remeshing process (zoom around $y^2 = 0$) for $\varepsilon = 10^{-6}$

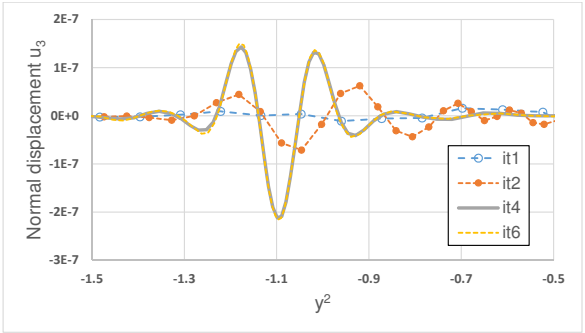

Figure 15. Case HP-H: Evolution of u_3^ε on the line $y^2 = -\frac{L}{2}$ during the remeshing process (zoom around $y^2 = -1$) for $\varepsilon = 10^{-6}$

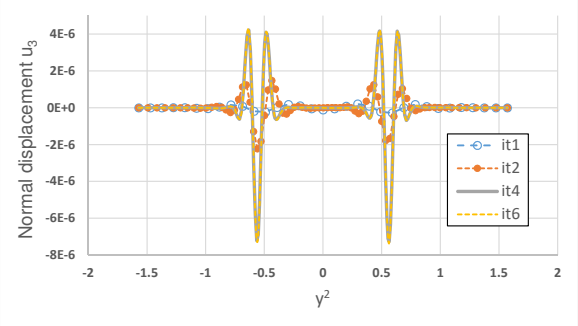

Figure 16. Case HP-H: Evolution of u_3^ε on the line $y^2 = 0$ during the remeshing process for $\varepsilon = 10^{-6}$

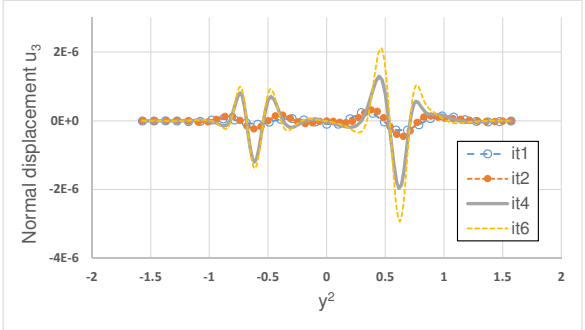

Figure 17. Case HP-H: Evolution of u_3^ε on the line $y^2 = \frac{L}{2}$ during the remeshing process for $\varepsilon = 10^{-6}$

4.2.2. *Results obtained for a relative thickness* $\varepsilon = 10^{-6}$

Let us now focus on the results of the computations obtained at the last iteration of the remeshing. The deformed shape of the shell is given on FIG. 18 with the Von Mises contours just under the upper surface (at 97.8% of the half-thickness).

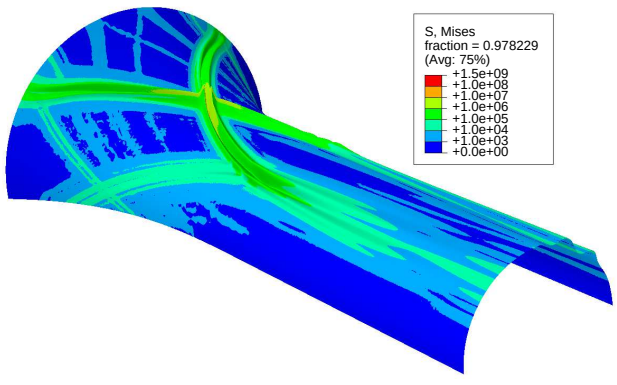

Figure 18. Case HP-H: Deformed shape (scale factor of 500) with Von Mises stress contours (just under the upper surface) for $\varepsilon = 10^{-6}$

On FIG. 18, we see that the singularity caused by the point force f^3 propagates along the two asymptotic lines AL_1 and AL_2 passing through the point P (see FIG. 8). The two singularities propagate also in the parabolic part. Moreover, we can observe a kind of reflection at $y^1 = 0$ along the curves AL'_1 and AL'_2. Let us investigate the propagation of these singularities more precisely by plotting the normal displacement u_3^ε on the lines $y^1 = -\frac{L}{2}$, $y^2 = 0$ and $y^1 = \frac{L}{2}$.

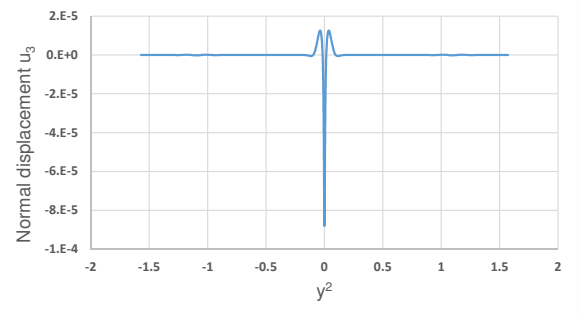

Figure 19. Case HP-H : Displacement u_3^ε on the line $y^1 = -\frac{L}{2}$ for $\varepsilon = 10^{-6}$

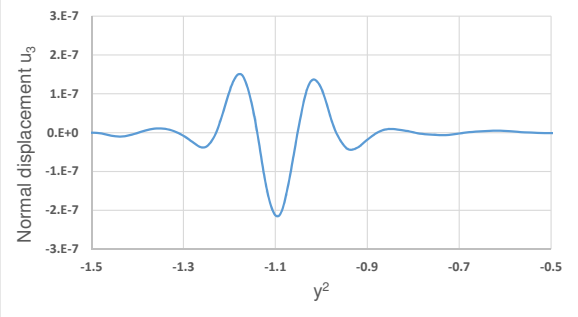

Figure 20. Case HP-H: Displacement u_3^ε on the line $y^1 = -\frac{L}{2}$ (zoom around $y^2 = -1$) for $\varepsilon = 10^{-6}$

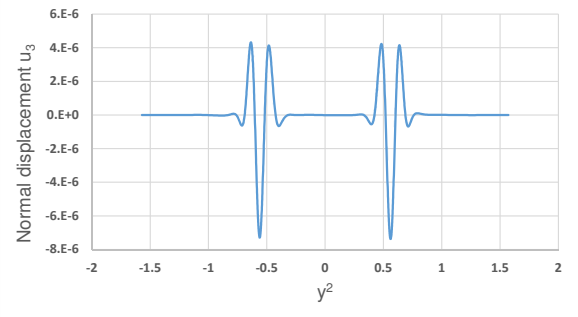

Figure 21. Case HP-H: Displacement u_3^ε on the line $y^1 = 0$ for $\varepsilon = 10^{-6}$

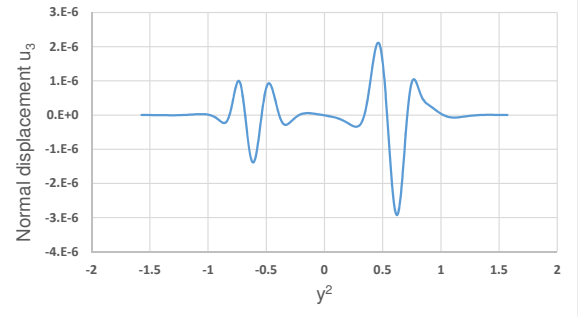

Figure 22. Case HP-H: Displacement u_3^ε on the line $y^2 = \frac{L}{2}$ for $\varepsilon = 10^{-6}$

In the case of hyperbolic shells, the displacement u_3^0 is two orders more singular than f^3. As the loading f^3 has a δ singularity, the displacement u_3^0 must have a $\delta^{(2)}$ singularity. Referring to FIG. 5, it corresponds to 3 main oscillations. That is what we can see on FIG. 19 at $y^2 = 0$. That singularity propagates along the two asymptotic lines AL_1 and AL_2 leading to two singularities which can be clearly seen at $y^1 = 0$ respectively around $y^2 \approx -0.5643$ and $y^2 \approx 0.5643$ (FIG. 21). These singularities propagate in the parabolic part along the asymptotic lines $y^2 \approx \pm 0.5643$ with a decreasing amplitude (FIG. 22). At $y^1 = 0$, we can see a kind of reflection: the two singularities arriving respectively at points P_1 and P_2 (along the two asymptotic lines coming from point P) are "reflected" along the second asymptotic lines passing through these two points (respectively AL'_1 and AL'_2, see FIG. 13). It can be observed on FIG. 20 where 3 oscillations appear around the point $(y^1 = -\frac{L}{2}; y^2 \approx -1.07)$.

Moreover, a pseudo-reflection as described in [14] occurs at $y^1 = -L/2$ at the boundary points P'_1 and P'_2 along the 2 asymptotic lines AL''_1 and AL''_2. It is a phenomenon specific to the hyperbolic shells and it will not be studied in the sequel.

Remark *The singularities propagating along AL'_1, AL'_2, AL''_1 and AL''_2 have a pseudo-reflection at the*

boundary $y^2 = -\pi/2$ or $y^2 = \pi/2$. And the "pseudo-reflected singularities" also reflect again if they reach another boundary in the hyperbolic part. The subsequent pseudo-reflections are difficult to detect because they are of a lower order and amplitude and they are hidden by the internal layers along respectively AL_2'', AL_1'', AL_2' and AL_1'.

Using the number of oscillations is not accurate enough to conclude about the order of the singularity. The "ideal function" (14) is an example and other examples of such functions could have a different number of oscillations but the same properties (amplitude tending to infinity with integral equal to 1). Moreover, it is difficult to see which oscillations are significant. To characterize more precisely these different singularities and especially their orders, we will now study their evolution during the singular perturbation process (when $\varepsilon \searrow 0$).

4.2.3. *Study of the singular perturbation process (when $\varepsilon \searrow 0$)*

The results obtained for the normal displacement u_3^ε numerically for $\varepsilon > 0$ play the role of (14) or one of its derivatives and tend to the limit solution u_3^0 (which is a distribution of the Dirac family (13)) as $\varepsilon \searrow 0$. Considering the properties of the Dirac family of paragraph 2.1, especially the thickness η of the layer and the amplitude of the singularities, it will enable us to determine the order of the singularities of the limit solution u_3^0 (see FIG. 5).

The normal displacement u_3^ε normalized for each relative thickness ε (by the maximum of its absolute value on the corresponding line) is plotted on FIG. 23 to FIG. 26 on different lines.

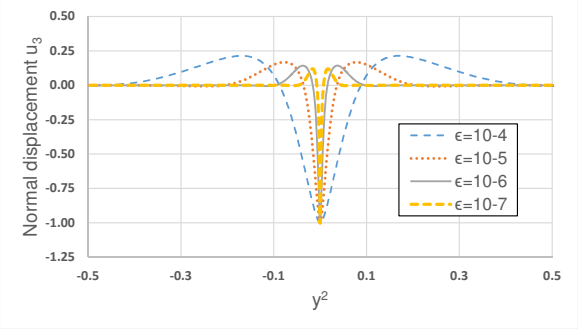

Figure 23. Case HP-H: Evolution of the normalized normal displacement $u_3/|u_3|_{max}$ on the line $y^2 = -L/2$ (zoom around $y^2 = 0$)

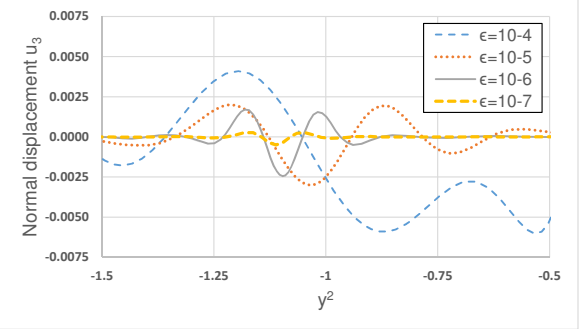

Figure 24. Case HP-H: Evolution of the normalized normal displacement $u_3/|u_3|_{max}$ on the line $y^2 = -L/2$ (zoom around $y^2 = -1$)

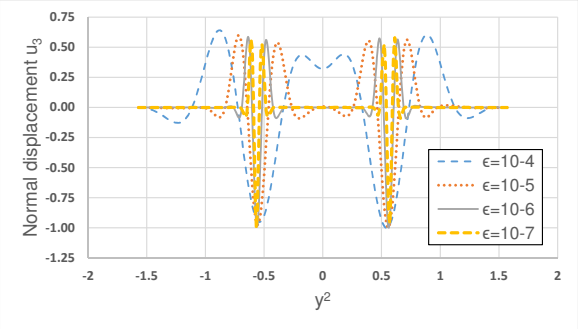

Figure 25. Case HP-H: Evolution of the normalized normal displacement $u_3/|u_3|_{max}$ on the line $y^2 = 0$

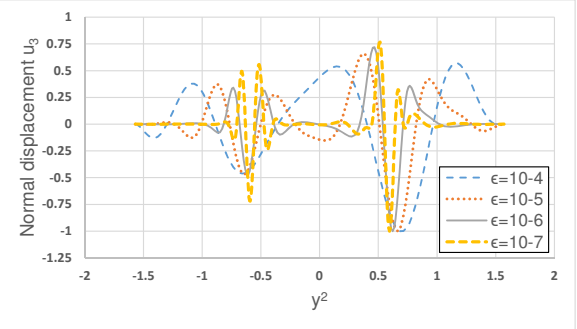

Figure 26. Case HP-H: Evolution of the normalized normal displacement $u_3/|u_3|_{max}$ on the line $y^2 = L/2$

When $\varepsilon \searrow 0$, we clearly see that the thickness of the singularities diminishes. In the same time, the amplitude of u_3^ε increases inside the layers: on line $y^1 = -L/2$ (FIG. 23), from $\varepsilon = 10^{-4}$ to $\varepsilon = 10^{-7}$, it was respectively 6.23 10^{-7}, 7.56 10^{-6}, 8.80 10^{-5} and 9.98 10^{-4}.

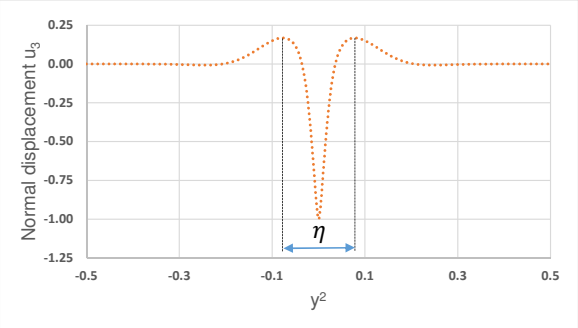

Figure 27. Measure of the layer thickness η on the line $y^1 = -L/2$

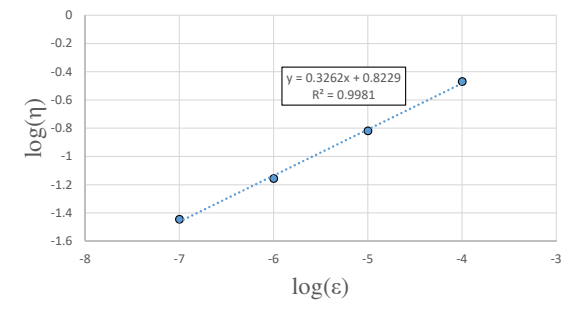

Figure 28. Case HP-H: Layer thickness with respect to ε on the line $y^1 = -L/2$

On each line ($y^1 = -L/2$, $y^1 = 0$, $y^1 = L/2$), we measured the thickness η (distance between 2 main peaks of the oscillations, see FIG. 27) and the maximal value of the displacement. Plotting them with respect to the relative thickness ε in a logarithmic scale like in the example in FIG. 28, and fitting the numerical results with a straight line, we find how the thickness and amplitude of each singularity evolve with respect to ε (Table 3). All the results are obtained with a coefficient of determination R^2 superior to 0.995.

position	thickness	amplitude	interpretation
$y^1 = -L/2$	$\mathcal{O}(\varepsilon^{0.3262})$	$\mathcal{O}(\varepsilon^{-1.0680})$	$\delta^{(2)}$
$y^1 = 0$	$\mathcal{O}(\varepsilon^{0.309})$	$\mathcal{O}(\varepsilon^{-0.9743})$	?
$y^1 = +L/2$	$\mathcal{O}(\varepsilon^{0.2531})$	$\mathcal{O}(\varepsilon^{-0.9593})$	$\delta^{(3)}$
$y^1 = -L/2$ (reflection)	$\mathcal{O}(\varepsilon^{0.3048})$	$\mathcal{O}(\varepsilon^{-0.9239})$	$\delta^{(2)}$

Table 3
Case HP-H: Evolution of the layer thicknesses and amplitudes of u_3^ε at different locations

Considering the theoretical results of Table 1, the displacement u_3^0 should be 2 orders more singular than the normal force f^3. Consequently, u_3^0 should have $\delta^{(2)}$ singularities along the asymptotic lines passing through P. As described on FIG. 5, this singularity has an amplitude in $1/\eta^3$, with η the layer thickness. In the case of hyperbolic shells, the layer thickness along asymptotic lines is of order $\eta = \mathcal{O}(\varepsilon^{1/3})$. So finally, the amplitude should vary in $\mathcal{O}(\varepsilon^{-1})$. We find coherent results for both the thickness and the amplitude on the line $y^1 = -L/2$.

Let us now characterize the singularity in the parabolic part. In the case of uniformly parabolic shells, the layer thickness of propagated singularities is of order $\eta = \mathcal{O}(\varepsilon^{1/4})$ (see Table 1). Thus the amplitude of a $\delta^{(2)}$ singularity propagating in the parabolic part should be of order $\mathcal{O}(\varepsilon^{-3/4})$. The layer thickness found is close to the theoretical result but the amplitude is not close to the order $\mathcal{O}(\varepsilon^{-3/4})$ even if it varies more slowly than in the hyperbolic part $\mathcal{O}(\varepsilon^{-0.9593})$. The singularity amplitude seems to vary in $1/\eta^4$ which correspond to a singularity in $\delta^{(3)}$.

At the transition, in $y^1 = 0$, the amplitude of the displacements and the layer thickness is between those of the hyperbolic and parabolic parts. We have a smooth transition for the layer thickness between the hyperbolic and parabolic parts.

The pseudo-reflected singularities along AL'_1 and AL'_2 are difficult to characterize. The results obtained for $\varepsilon = 10^{-4}$ were not used for the reflection in the results of Table 3 because the layers are too large and interact with the layers around AL_1 and AL_2. If we remove also the results obtained for $\varepsilon = 10^{-7}$ which may suffer from locking, we get $\eta = \mathcal{O}(\varepsilon^{0.3136})$ and an amplitude in $\mathcal{O}(\varepsilon^{-0.9713})$: it seems that theirs properties are closed to the ones observed at the transition at $y^1 = 0$.

4.3. *Normal force $\tilde{f}^3$ applied in the parabolic part (Case HP-P)*

In this part, let us consider that the normal force $\tilde{f}^3$, normal to the surface is applied at the point $P' = (+\frac{L}{2}, 0)$ in the plane of parameters, in the parabolic part. The asymptotic lines passing through point P' are plotted on FIG. 29 in the plane of parameters (y^1, y^2).

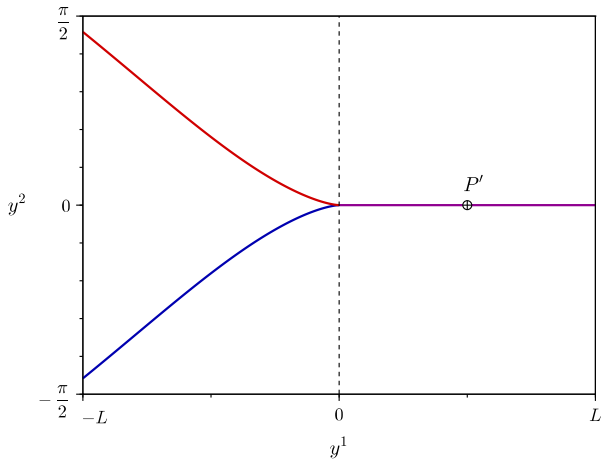

Figure 29. Case HP-P: The asymptotic lines passing trough the point P' in the plane of parameters.

The deformed shape obtained for $\varepsilon = 10^{-6}$ is given on FIG. 30.

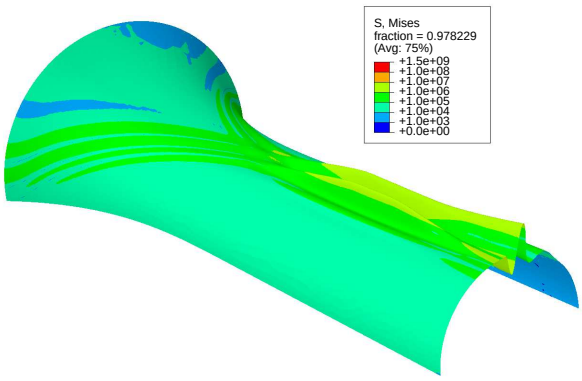

Figure 30. Case HP-P: Deformed shape (scale factor of 57) with Von Mises stress contours (just under the upper surface) for $\varepsilon = 10^{-6}$

When the normal force f^3 is singular along an asymptotic line of a parabolic shell (that's necessarily the case for a point force), the normal displacement u_3^0 is 4 orders more singular than the force (Table 1). As f^3 has a singularity in δ, u_3^0 has a singularity in $\delta^{(4)}$ corresponding to 5 oscillations (FIG. 31). The singularity propagates along the asymptotic line $y^2 = 0$ up to the point $(0, 0)$ (FIG. 32). At $y^1 = 0$, the singularity is

transmitted in the hyperbolic part ($y^1 < 0$) and propagates along the two asymptotic lines (FIG. 33) passing through the point $(0, 0)$.

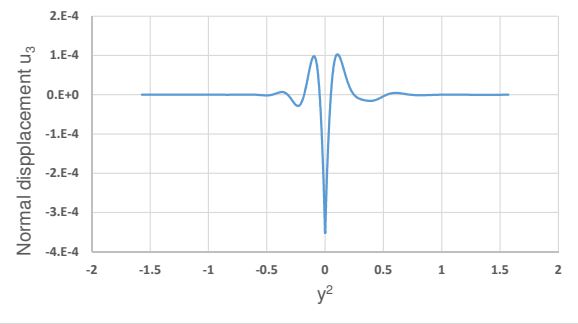

Figure 31. Case HP-P: Displacement u_3^ε on the line $y^2 = \frac{L}{2}$

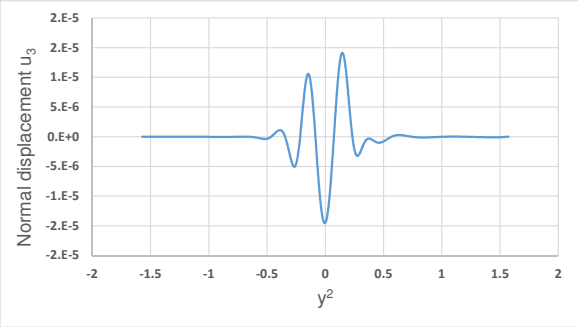

Figure 32. Case HP-P: Displacement u_3^ε on the line $y^1 = 0$

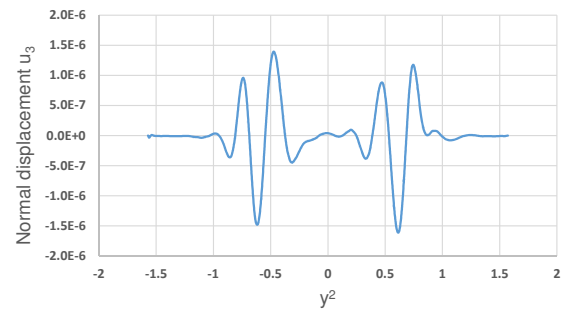

Figure 33. Case HP-P: Displacement u_3^ε on the line $y^1 = -\frac{L}{2}$

To determine the order of the singularities, we study the singular perturbation process. Computations are carried out with relative thicknesses $\varepsilon = 10^{-4}$, 10^{-5}, 10^{-6} and 10^{-7}. The results obtained allow to estimate the variation of the layer thickness η and the amplitude of the singularities. These estimations are presented in Table 4 with a coefficient of determination $R^2 > 0.998$.

position	thickness	amplitude	interpretation
$y^1 = L/2$	$\mathcal{O}(\varepsilon^{0.2635})$	$\mathcal{O}(\varepsilon^{-1.2353})$	$\delta^{(4)}$
$y^1 = 0$	$\mathcal{O}(\varepsilon^{0.2563})$	$\mathcal{O}(\varepsilon^{-1.0066})$	?
$y^1 = -L/2$	$\mathcal{O}(\varepsilon^{0.3397})$	$\mathcal{O}(\varepsilon^{-0.9992})$	$\delta^{(2)}$

Table 4
Case HP-P: Layer thicknesses and amplitudes for u_3^ε at different locations (force in the parabolic part)

The normal displacement u_3^0 should have $\delta^{(4)}$ singularities along the asymptotic lines passing through P. This singularity has an amplitude in $1/\eta^5$, with η the layer thickness. In the case of parabolic shells, the layer thickness along asymptotic lines is of order $\eta = \mathcal{O}(\varepsilon^{1/4})$. Consequently, the amplitude should be of order $\mathcal{O}(\varepsilon^{-5/4})$. The singularity in the parabolic part is clearly a $\delta^{(4)}$ as predicted by the theory with an amplitude very close to $\mathcal{O}(\varepsilon^{-5/4})$. The layer thickness evolves from $\eta = \mathcal{O}(\varepsilon^{1/4})$ in the parabolic part to $\eta = \mathcal{O}(\varepsilon^{1/3})$ in the hyperbolic part. From this numerical results, we can conclude that the singularity is in $\delta^{(4)}$ in the parabolic part and propagates as 2 singularities in $\delta^{(2)}$ in the hyperbolic part (since the amplitude is in $1/\eta^3$).

5. Hyperbolic-Elliptic shell

5.1. *The shell considered and its geometrical properties*

We now address the case of a hyperbolic/elliptic shell. The middle surface of the shell is defined by the local mapping (Ω, Ψ) given in (15) with $\Omega = [-L, \rho] \times [-\pi/2, \pi/2]$ and

$$\begin{cases} R(y^1) = \rho\left(1 - \left(y^1/L\right)^3\right) & \text{for } \; y^1 \epsilon\, [-L, 0[\\ \\ R(y^1) = \sqrt{\rho^2 - (y^1)^2} & \text{for } \; y^1 \epsilon\, [0, \rho] \end{cases} \tag{22}$$

The part corresponding to $y^1 < 0$ is hyperbolic whereas the part of the surface corresponding to $y^1 \geq 0$ is elliptic. The elliptic part corresponds to a quarter of sphere (see FIG. 34). The characteristic length of the HE shell is taken as $L_C = 0.14452\ m$ (the length of the curve $y^2 = 0$).

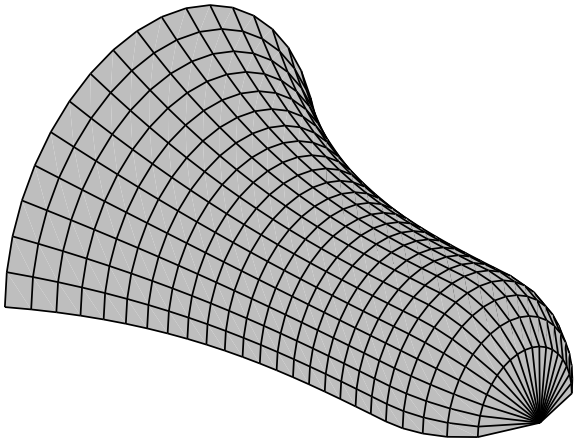

Figure 34. Middle surface of the HE shell

The data used for this problem are the same as for the HP shell and referenced in the Table 2.

Boundary conditions
The shell is clamped at all its boundary to ensure that the shell is inhibited in the hyperbolic part and well-inhibited in the elliptic part [20].

Loading
Two cases will be addressed. For both cases, a normal point force, proportional to the relative thickness is applied $\tilde{f}^3 = -0.01 \times \varepsilon\ N$ (corresponding to $f^3 = -0.01\ N$ in equation (4)), is applied, in the hyperbolic part for the case HE-H or in the elliptic case for the case HE-E.

Remark *The problem is symmetrical with respect to the plane* $y = 0$.

5.2. *Normal force $\tilde{f}^3$ applied in the hyperbolic part (Case HE-H)*

Let us consider that a force $\tilde{f}^3$, normal to the surface is applied at the point $P = (-L/2, 0)$ in the plane of parameters.

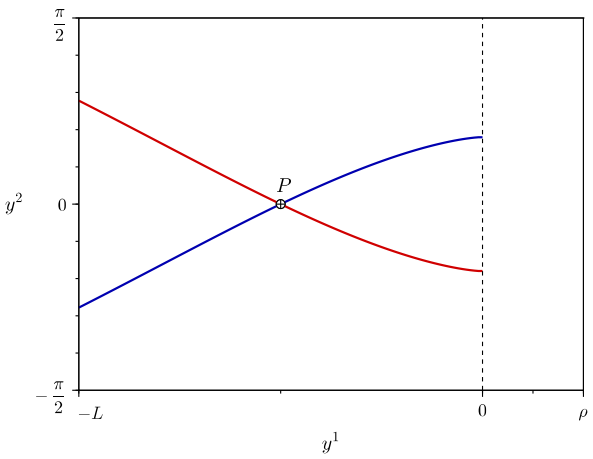

Figure 35. Case HE-H: The asymptotic lines passing through the point P in the plane of parameters.

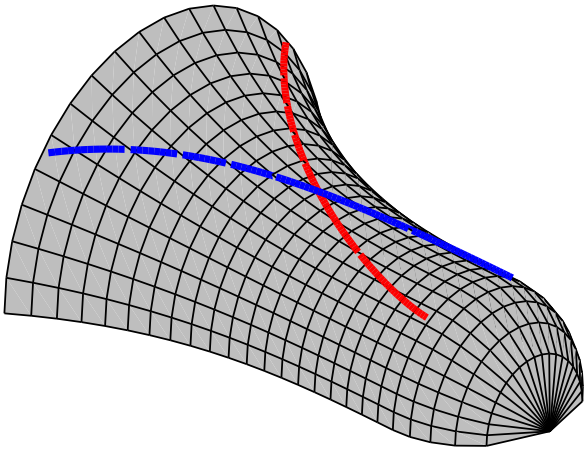

Figure 36. Case HE-H: The asymptotic lines passing through the point $\Psi(-L/2, 0)$ in the 3D space.

In the hyperbolic part, the asymptotic lines passing through point P are the same as in the HP-H case (section section 4.2). However, the asymptotic lines stop at $y^1 = 0$ since there is no asymptotic line in the elliptic part.

The deformed shape of the shell obtained for $\varepsilon = 10^{-6}$ with the last mesh (FIG. 37) of the remeshing process is plotted on FIG. 38.

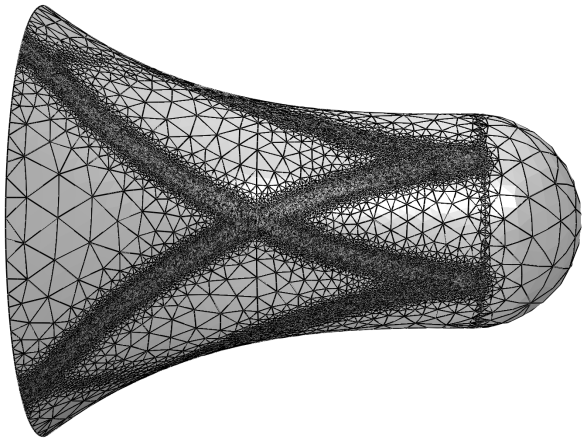

Figure 37. Case HE-H: Mesh at the last iteration (261,746 elements)

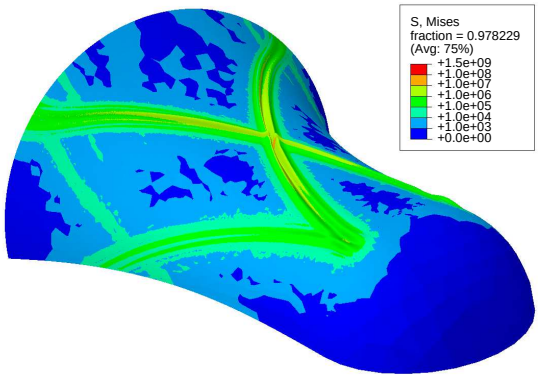

Figure 38. Case HE-H: Deformed shape (scale factor of 65) with Von Mises stress contours (just under the upper surface)

Like in the case HP-H, the singularity caused by the point force f^3 propagates along the two asymptotic lines passing through the point P (see FIG. 36) leading to two singularities which also reflect at $y^1 = 0$. Let us investigate the propagation more precisely by plotting the normal displacement u_3^ε on the lines $y^1 = -L/2$, $y^2 = 0$.

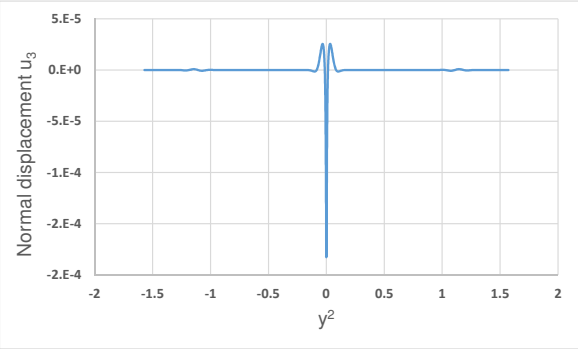

Figure 39. Case HE-H: Displacement u_3^ε on the line $y^1 = -\frac{L}{2}$

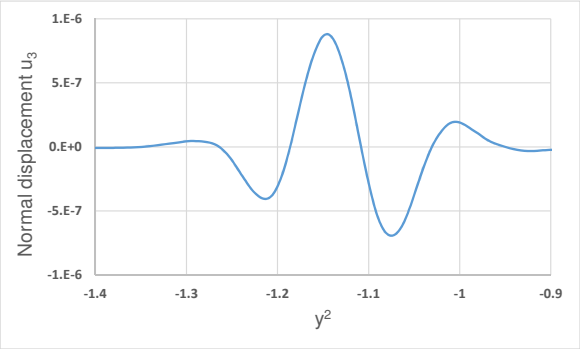

Figure 40. Case HE-H: Displacement u_3^ε on the line $y^1 = -\frac{L}{2}$ (zoom around $y^2 = -1.15$)

In the hyperbolic part, the same singularity apparently in $\delta^{(2)}$ is observed (FIG. 39). Arriving at the boundary between hyperbolic and elliptic parts (corresponding to the line $y^1 = 0$ in the plane of parameters), the singularity is still visible at the transition line $y^1 = 0$ (FIG. 41) and does not propagate in the elliptic part (FIG. 42) but reflects and propagates along the other asymptotic line arriving at the 2 points $(0, y^2 \approx \pm 0.5643)$ (FIG. 40). The oscillations visible in the elliptic part are due to the boundary layers present in $y^2 = \pm\pi/2$.

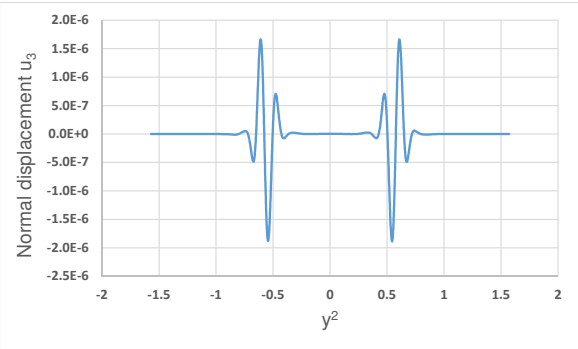

Figure 41. Case HE-H: Displacement u_3^ε on the line $y^1 = 0$

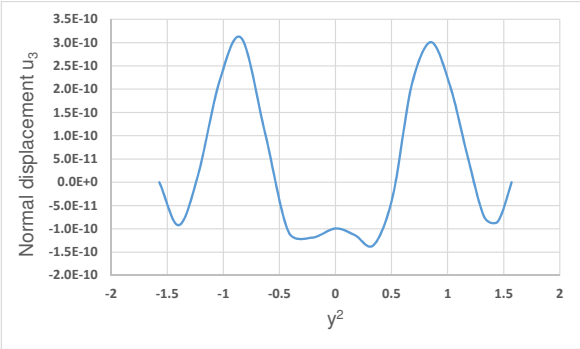

Figure 42. Case HE-H: Displacement u_3^ε on the arc of the circle passing through point P''

position	thickness	amplitude	interpretation
$y^1 = -L/2$	$\mathcal{O}(\varepsilon^{0.3327})$	$\mathcal{O}(\varepsilon^{-1.0656})$	$\delta^{(2)}$
$y^1 = 0$	$\mathcal{O}(\varepsilon^{0.3257})$	$\mathcal{O}(\varepsilon^{-0.9273})$	?
$y^1 = -L/2$ (reflection)	$\mathcal{O}(\varepsilon^{0.3163})$	$\mathcal{O}(\varepsilon^{-0.9721})$	$\delta^{(2)}$

Table 5
Case HE-H: Layer thicknesses and amplitudes for u_3^ε at different locations

The results for $\varepsilon = 10^{-7}$ were discarded because the symmetry with respect to the plane $y = 0$ was lost. All the layers thicknesses are closed to $\mathcal{O}(\varepsilon^{1/3})$ and the amplitudes closed to $\mathcal{O}(\varepsilon^{-1})$. So it seems that all the singularities of u_3^0 and especially the ones reflected are in $\delta^{(2)}$. Contrary to the "pseudo-reflection" phenomenon [11], the reflection seems to be here total and conserves the order of the singularity.

5.3. *Normal force $\tilde{f}^3$ applied in the elliptic part (Case HE-E)*

In this part, let us consider that the force $\tilde{f}^3$, normal to the surface is applied at the point $P'' = (\sqrt{2}\rho/2, 0)$ in the plane of parameters. The remeshing just consists in refining the mesh around point P''. The deformed shape obtained for $\varepsilon = 10^{-6}$ is given on FIG. 43.

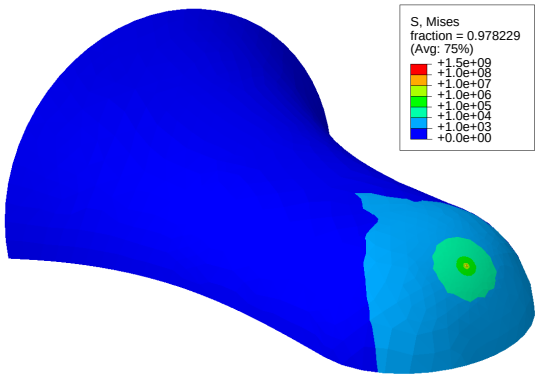

Figure 43. Case HE-E: Deformed shape (scale factor of 750) with Von Mises stress contours (just under the upper surface)

No asymptotic line existing in the elliptic part, there is no propagation of the singularity. Moreover, there is no *logarithmic singularities* because the shell is a sphere and the two principal curvatures are equal at point P'' [16].

6. Parabolic-Elliptic shell

6.1. *The shell considered and its geometrical properties*

The last example deals with a parabolic/elliptic shell. The middle surface of the shell is defined by the local mapping (Ω, Ψ) given in (15) with $\Omega = [-L, \rho] \times [-\pi/2, \pi/2]$ and

$$\begin{cases} R(y^1) = \rho & \text{for } \; y^1 \epsilon \, [-L, 0[\\ \\ R(y^1) = \sqrt{\rho^2 - (y^1)^2} & \text{for } \; y^1 \epsilon \, [0, \rho] \end{cases} \tag{23}$$

The part corresponding to $y^1 < 0$ is parabolic whereas the part of the surface corresponding to $y^1 \geq 0$ is elliptic. The two parts of the surface are respectively to a half cylinder and a quarter of sphere (see FIG. 44). The characteristic length is taken as $L_C = 0.13927\ m$ (length of the curve $y^2 = 0$). The numerical data used is summarised in Table 2.

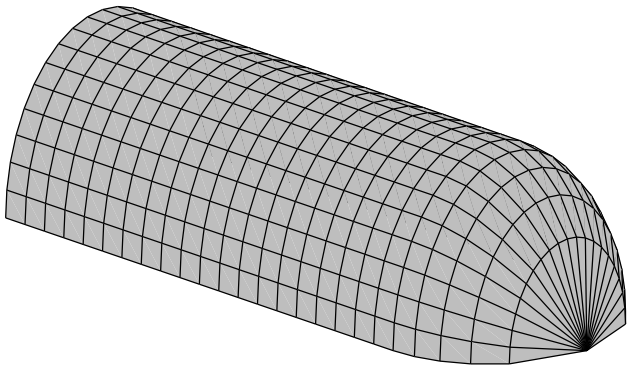

Figure 44. Middle surface of the PE shell

The asymptotic lines are the lines $y^2 = constant$ in the parabolic part and no real asymptotic line exist in the elliptic part.

Boundary conditions
The shell is clamped at all its boundary to ensure that the shell is inhibited in the parabolic part and well-inhibited in the elliptic part.

Loading
Two cases will be addressed. For both cases, a normal point force, proportional to the relative thickness is applied $\tilde{f}^3 = -0.01 \times \varepsilon\ N$ corresponding to $f^3 = -0.01\ N$ in equation (4)), is applied, in the parabolic part for the case PE-P or in the elliptic case for the case PE-E.

Remark *The problem is symmetrical with respect to the plane* $y = 0$.

6.2. *Normal force* $\tilde{f}^3$ *applied in the parabolic part (Case PE-P)*

Let us consider that the force $\tilde{f}^3$, normal to the surface is applied at the point $P = (-\frac{L}{2}, 0)$ in the plane of parameters, in the parabolic part. There is only one asymptotic line passing through point P, the generator of the cylinder of equation $y^2 = 0$.

The deformed shape of the shell obtained for $\varepsilon = 10^{-6}$ with the mesh of the last iteration (FIG. 45) is plotted on FIG. 46. The singularity is limited to the parabolic part. No propagation occurs in the elliptic part.

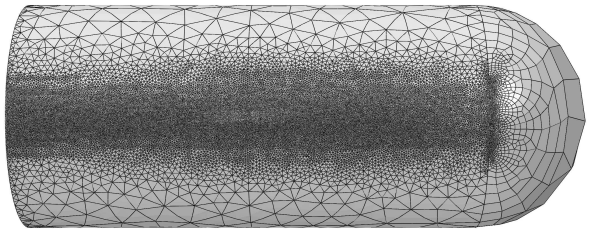

Figure 45. Case PE-P: Mesh at the last iteration (100,768 elements)

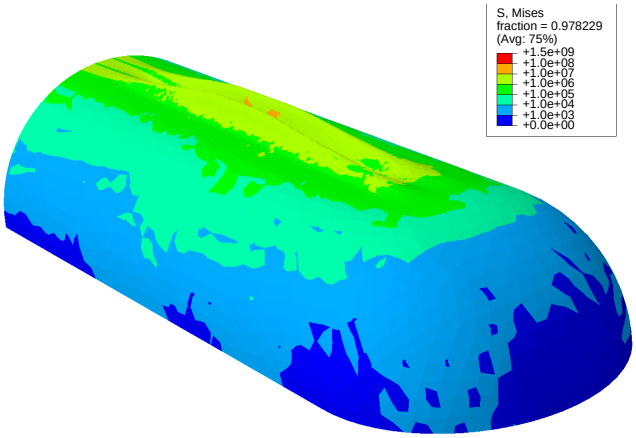

Figure 46. Case PE-P: Deformed shape (scale factor of 17) with Von Mises stress contours (just under the upper surface)

In the parabolic part, the singularity in $\delta^{(4)}$ (FIG. 47) caused by the point force f^3 propagates along the asymptotic line $y^1 = 0$ up to the point $(0, 0)$ (FIG. 48). This singularity does not propagate in the elliptic part (FIG. 49) and does not reflect since there is no other asymptotic line passing through the point $(0, 0)$.

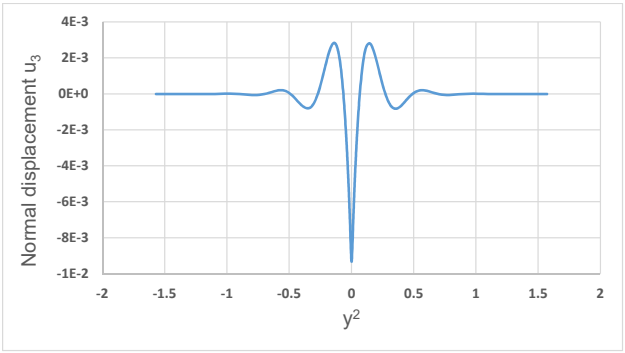

Figure 47. Case PE-P: Displacement u_3^ε on the line $y^1 = -\frac{L}{2}$

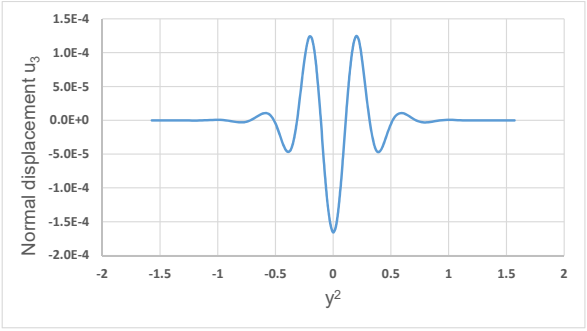

Figure 48. Case PE-P: Displacement u_3^ε on the line $y^1 = 0$

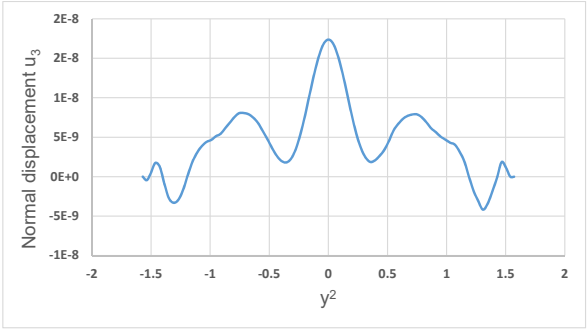

Figure 49. Case PE-P: Displacement u_3^ε on the half perimeter of the quarter sphere passing through the point $(0, \sqrt{2}\rho/2)$

The numerical computations show here the classical results for parabolic shells [12]. There are no interaction between the parabolic part and the elliptic part in terms of singularities.

6.3. *Normal force $\tilde{f}^3$ applied in the elliptic part (Case PE-E)*

In this part, let us consider that the force $\tilde{f}^3$, normal to the surface is applied at the point $P'' = (\sqrt{2}\rho/2, 0)$ in the plane of parameters, in the elliptic part. The remeshing consists here again in refining the mesh around point P''. The deformed shape obtained of $\varepsilon = 10^{-6}$ is plotted on FIG. 50.

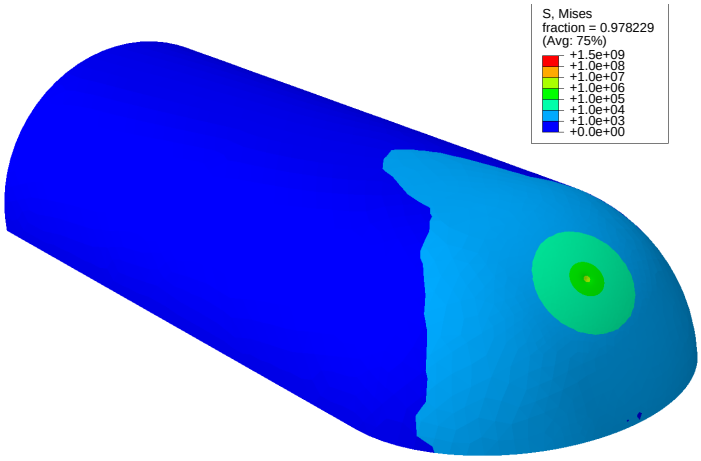

Figure 50. Case PE-E: Deformed shape (scale factor of 750) with Von Mises stress contours (just under the upper surface)

No asymptotic line existing in the elliptic part, there is no propagation of the singularities in the elliptic part and consequently no singularity in the parabolic part. The results are very similar to the ones obtained in the case HE-E.

7. Conclusion

In this paper, we performed numerical computations using adaptive meshes to study the propagation of singularities in thin elastic shells having a non-uniform nature (hyperbolic-parabolic, hyperbolic-elliptic or parabolic-elliptic). The most interesting cases are the shells with a hyperbolic part.
When a singular force is applied in a hyperbolic part, the singularity of the normal displacement u_3^0 classically propagates along two asymptotic lines. If the second part of the shell is parabolic, the singularities propagate in the parabolic part along two distinct asymptotic lines with what seems to be one order higher. If the second part is elliptic, the singularities do not propagate in the elliptic part as no asymptotic line exist. In both cases, the singularity reflects at the boundary between both parts in the hyperbolic part following the second asymptotic line. It seems that the reflected singularity keeps the same order as the original one. In the HP case, the original and reflected singularities add up to give a higher order singularity in the parabolic part. In the HE case, they balance to give no singularity in the elliptic part.

In the HP case, if the singular force is applied in the parabolic part, the normal displacement is 4 orders more singular in the parabolic part and classically propagate along the asymptotic line. It then propagates in the hyperbolic part along the 2 asymptotic lines (apparently) losing 2 orders.
Finally, for the other cases, no new results were highlighted.

A theoretical study should be carried out to prove the observed results but it is not clear up to now how to proceed since we can not use the well-adapted coordinate system based on the characteristic lines of the membrane system (11). Indeed, we chose a problem with smooth transition between both part of the shell. The consequence is that the two families of characteristic lines in the hyperbolic part tend to become the same at the boundary between the 2 parts. Consequently, the coordinate system based on the two characteristic lines is unusable at the transition. To avoid this problem, we could study the same kind of problem but with a fold (the normal to the shell would not be continuous at the transition). But, it is not sure that the same kind of results would be obtained. Moreover, the study was limited to revolution shells and it would be interesting to study more general types of shells.
For shells with elliptic part, a study could also be carried out when a part of the boundary of the shell is free. There should be situations where the shell is not well-inhibited leading to complexification phenomena that may propagate in the non-elliptic part of the shell.

References

[1] J. Stoker, Differential geometry. 1969, New York Interscience.

[2] E. Sanchez-Palencia, Statique et dynamique des coques minces, II- Cas de flexion pure inhibée. approximation membranaire, Comptes rendus de l'Académie des sciences. Série 1, Mathématique 309 (1989) 531–537.

[3] E. Sanchez-Palencia, Statique et dynamique des coques minces, I- Cas de flexion pure non inhibée, Comptes rendus de l'Académie des sciences. Série 1, Mathématique 309 (1989) 411–417.

[4] W. T. Koiter, The Theory of Thin Elastic Shells: Proc. of Symposium, North-Holland, 1960.

[5] P. G. Ciarlet, V. Lods, Asymptotic analysis of linearly elastic shells. III. Justification of Koiter's shell equations, Archive for Rational Mechanics and Analysis 136 (1996) 191–200.

[6] D. Chapelle, K.-J. Bathe, The finite element analysis of shells-fundamentals, Springer Science & Business Media, 2010.

[7] M. Bernadou, P. G. Ciarlet, Sur l'ellipticité du modele linéaire de coques de W. T. Koiter (1976) 89–136.

[8] D. Choi, On geometrical rigidity of surfaces., Mathematical Models and Methods in Applied Sciences 07 (1997) 507–555.

[9] J. Sanchez-Hubert, E. Sanchez-Palencia, Coques élastiques minces, Masson, 1997.

[10] E. Sanchez-Palencia, O. Millet, F. Béchet, Thin Elastic Shells-Computing and Asymptotics, Springer, 2010.

[11] P. Karamian, J. Sanchez-Hubert, Boundary layers in thin elastic shells with developable middle surface, European Journal of Mechanics-A/Solids 21 (1) (2002) 13–47.

[12] F. Béchet, O. Millet, E. Sanchez-Palencia, Adaptive and anisotropic mesh strategy for thin shell problems. Case of inhibited parabolic shells, International Journal of Solids and Structures 46 (3) (2009) 534 – 556.

[13] C. De Souza, F. Béchet, D. Leguillon, E. Sanchez-Palencia, Anisotropic adaptive mesh procedure for computing very thin hyperbolic shells, BIT Numerical Mathematics 48 (2) (2008) 357–387.

[14] P. Karamian-Surville, J. Sanchez-Hubert, E. Sanchez Palencia, Pseudo-reflection phenomena for singularities in thin elastic shells, Mathematical methods in the applied sciences 26 (17) (2003) 1451–1485.

[15] P. Karamian-Surville, The refraction phenomenon of singularities in thin elastic shells with developable mid-surface in presence of rigid folds: Case of parabolic shells, European Journal of Mechanics - A/Solids 55 (Supplement C) (2016) 12 – 34.

[16] F. Béchet, E. Sanchez-Palencia, O. Millet, Computing singular perturbations for linear elliptic shells, Computational Mechanics 42 (2) (2008) 287–304.

[17] J. Pitkaranta, E. Sanchez-Palencia, On the asymptotic behaviour of sensitive shells with small thickness, Comptes Rendus de l'Académie des Sciences-Series IIB-Mechanics-Physics-Chemistry-Astronomy 325 (3) (1997) 127–134.

[18] K.-J. Bathe, D. Chapelle, P.-S. Lee, A shell problem 'highly sensitive'to thickness changes, International journal for numerical methods in engineering 57 (8) (2003) 1039–1052.

[19] C. A. D. Souza, Évariste Sanchez-Palencia, Complexification phenomenon in an example of sensitive singular perturbation, Comptes Rendus Mécanique 332 (8) (2004) 605 – 612.

[20] F. Béchet, E. Sanchez-Palencia, O. Millet, Singular perturbations generating complexification phenomena for elliptic shells, Computational mechanics 43 (2) (2009) 207–221.

[21] V. ABAQUS, 6.14 documentation, Dassault Systemes Simulia Corporation.

[22] B. Budiansky, J. L. Sanders, On the 'best' first-order linear shell theory, The Prager Anniversary Volume-Progress in Applied Mechanics (1963) 129–140.

[23] F. Béchet, E. Sanchez-Palencia, O. Millet, Singularities in shell theory: Anisotropic error estimates and numerical simulations, Computer Methods in Applied Mechanics and Engineering 199 (21) (2010) 1326 – 1341.